ORIGINAL RESEARCH
published: 25 January 2022
doi: 10.3389/fphy.2021.822694

Controlled Bistable Transmission Non-Reciprocity in a Four-Mode Optomechanical System

Bo Jiang[1], *Dong Yan*[2], *Jing Wang*[3]*, *Dezhan Qu*[4] *and Jin-Hui Wu*[1]*

[1]Center for Quantum Sciences and School of Physics, Northeast Normal University, Changchun, China, [2]School of Science, Changchun University, Changchun, China, [3]College of Physics, Tonghua Normal University, Tonghua, China, [4]School of Information Science and Technology, Northeast Normal University, Changchun, China

We examine the bistable transmission non-reciprocity in a four-mode optomechanical system, where a mechanical oscillator interacts with one of three coupled optical cavities so as to generate an asymmetric optomechanical non-linearity. Two transmission coefficients in opposite directions are found to exhibit non-reciprocal bistable behaviors due to this asymmetric optomechanical non-linearity as the impedance-matching condition is broken for a not too weak input field. Such a bistable transmission non-reciprocity can be well manipulated to exhibit reversible higher isolation ratios in tunable wider ranges of the input field power or one cavity mode detuning by modulating relevant parameters like optical coupling strengths, optomechanical coupling strengths, and mechanical frequencies. This optomechanical system provides a flexible platform for realizing transmission non-reciprocity of weal light signals and may be extended to optical networks with more coupled cavities.

Keywords: transmission non-reciprocity, bistable non-linearity, cavity optomechanics, impedance-matching breaking, optical isolation

OPEN ACCESS

Edited by:
Hui Yan,
South China Normal University, China

Reviewed by:
Keyu Xia,
Nanjing University, China
Jianming Wen,
Kennesaw State University, United States

Correspondence:
Jing Wang
pwl1207wj@163.com
Jin-Hui Wu
jhwu@nenu.edu.cn

Specialty section:
This article was submitted to Quantum Engineering and Technology, a section of the journal Frontiers in Physics

Received: *26 November 2021*
Accepted: *20 December 2021*
Published: *25 January 2022*

Citation:
Jiang B, Yan D, Wang J, Qu D and Wu J-H (2022) Controlled Bistable Transmission Non-Reciprocity in a Four-Mode Optomechanical System. Front. Phys. 9:822694. doi: 10.3389/fphy.2021.822694

1 INTRODUCTION

Cavity optomechanics, focusing on enhanced radiation pressure interactions between light fields and mechanical motions, has attracted extensive experimental and theoretical interests owing to its wide applications in processing quantum information, measuring weak signals, and developing new devices [1–9]. Various optomechanical systems have been proposed and fabricated to realize non-trivial tasks and interesting phenomena, such as entanglement generation between cavity and mechanical modes [10–15], ground-state cooling of mechanical resonators [16–20], optomechanically induced transparency (OMIT) and absorption (OMIA) [21–26], Bell non-locality verification [27], parity-time (PT) symmetry-breaking chaos [28], and tumor structural imaging [29]. We note in particular that optomechanical systems can provide an effective avenue for implementing non-reciprocal devices, like isolators and circulators, required in constructing all-optical communication networks [30–34].

Non-reciprocal devices promise the transmission of signals in one direction while blocking those propagating in the opposite direction and can be utilized to avoid unwanted interference of signals and protect optical sources and systems from noises [35–42]. Breaking reciprocity or time reversal symmetry is typically accomplished with magneto-optical effects [43–45] and has resulted in the emergence of new physics such as topologically protected one-way photonic edge modes [46] and non-reciprocal behaviors in giant atom systems [47, 48]. Unfortunately, magneto-optical effects are not present in standard optoelectronic materials including most metals and semiconductors and may

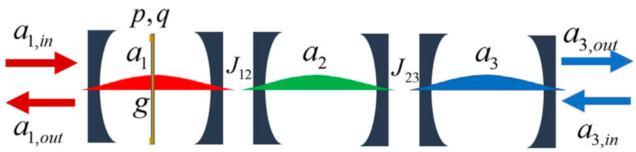

FIGURE 1 | (Color online) Schematic of an optomechanical system consisting of three cavities described by optical modes a_1, a_2, and a_3 as well as a membrane described by position q and momentum p. This system could be driven by an input field $a_{1,in}$ and exhibit an output field $a_{3,out}$, or driven by an input field $a_{3,in}$ and exhibit an output field $a_{1,out}$. Here, g denotes the optomechanical coupling strength, while J_{lk} represents the coupling strength between optical modes a_l and a_k.

result in crosstalk and other problems hampering on-chip implementations. This is why non-magnetic approaches for achieving optical non-reciprocity have been extensively studied with significant advances, for example, in chiral atomic systems [49–51] and optomechanical systems [30–34]. The latter includes, for instance, a three-mode optomechanical system with additional gain in one cavity [31] and a two-cavity optomechanical system with a blue-detuned driving [32].

Coupled micro-cavities are essential elements for constructing quantum information networks in that they are scalable via mode swapping or fiber coupling, compatible with mechanical oscillators and other elements, and easy to be controlled by driving fields. With this consideration, here we extend previous works [30–34] to seek more flexible manipulations on optical non-reciprocity by investigating a four-mode optomechanical system with three optical cavities and one mechanical oscillator. This system is found to exhibit an asymmetric optomechanical non-linearity, which then result in staggered bistable behaviors of two opposite-direction transmission coefficients, under the broken impedance-matching condition. Numerical results show in particular that quite a few parameters can be modulated on demand to manipulate, in different ways, the upper and lower stable branches of both transmission coefficients. This allows us to tune and widen non-reciprocal ranges in terms of the input power or a cavity detuning on the one hand, while improve isolation ratio and reverse isolation direction with respect to transmission coefficients on the other hand.

2 MODEL AND EQUATIONS

We consider a cavity optomechanical system consisting of three optical modes described by annihilation operators a_1, a_2, and a_3 and a mechanical mode described by position operator q and momentum operator p, as shown in **Figure 1**. These optical and mechanical modes exhibit frequencies ω_1, ω_2, ω_3, and ω_m, respectively. The $2nd$ optical mode is coupled to the $1st$ optical mode with strength J_{12}, while to the $3rd$ optical mode with strength J_{23}, in a linear way controlled via the in-between waveguide or fiber. The mechanical mode is coupled only to the $1st$ optical mode with single-photon optomechanical coupling strength g. A driving field of frequency ω_d is applied to excite the $1st$ optical mode with annihilation operator $a_{1,in}$ or the $3rd$ optical mode with annihilation operator $a_{3,in}$. With these considerations, we can write down the following Hamiltonian ($\hbar = 1$):

$$\begin{aligned} H = {} & \omega_1 a_1^\dagger a_1 + \omega_2 a_2^\dagger a_2 + \omega_3 a_3^\dagger a_3 + \frac{1}{2}\omega_m \left(p^2 + q^2\right) \\ & + g a_1^\dagger a_1 q + J_{12}\left(a_1^\dagger a_2 + a_2^\dagger a_1\right) + J_{23}\left(a_2^\dagger a_3 + a_3^\dagger a_2\right) \\ & + i\sqrt{\gamma_{1,e}}\left(a_1^\dagger a_{1,in} e^{-i\omega_d t} - a_1 a_{1,in}^\dagger e^{i\omega_d t}\right) \\ & + i\sqrt{\gamma_{3,e}}\left(a_3^\dagger a_{3,in} e^{-i\omega_d t} - a_3 a_{3,in}^\dagger e^{i\omega_d t}\right), \end{aligned} \tag{1}$$

where $\gamma_{j,e}$ has been taken as the coupling constant to the driving field, that is, the external decay rate, of the jth optical mode. It is worth noting that the jth optical mode also exhibits an intrinsic decay rate $\gamma_{j,i}$ so that its total decay rate turns out to be $\gamma_j = \gamma_{j,i} + \gamma_{j,e}$. Then we can define $\eta_j = \gamma_{j,e}/\gamma_j$ as an effective coupling ratio with $\eta_j = 0$ denoting a vanishing coupling, while $\eta_j = 1$ denoting the maximal coupling. To be more specific, our optomechanical system may be implemented either with a vibrational membrane coupled to one of three Fabry-Pérot cavities, or with an optomechanical crystal coupled to one of three photonic crystal cavities [52].

In the rotating frame of the driving frequency ω_d, it is viable to attain from the Hamiltonian in **Eq. 1** the following quantum Langevin equations (QLEs):

$$\begin{aligned} \partial_t a_1 &= -(\gamma_1/2 + i\Delta_1)a_1 - igqa_1 - iJ_{12}a_2 \\ &\quad + \sqrt{\gamma_{1,e}}a_{1,in} + \sqrt{\gamma_{1,i}}a_{1,vac}, \\ \partial_t a_2 &= -(\gamma_2/2 + i\Delta_2)a_2 - iJ_{12}a_1 - iJ_{23}a_3 \\ &\quad + \sqrt{\gamma_{2,i}}a_{2,vac}, \\ \partial_t a_3 &= -(\gamma_3/2 + i\Delta_3)a_3 - iJ_{23}a_2 \\ &\quad + \sqrt{\gamma_{3,e}}a_{3,in} + \sqrt{\gamma_{3,i}}a_{3,vac}, \\ \partial_t q &= \omega_m p, \\ \partial_t p &= -\omega_m q - g a_1^\dagger a_1 - \gamma_m p + \xi, \end{aligned} \tag{2}$$

where $\Delta_j = \omega_j - \omega_d$ is defined as the detuning of the jth optical mode to the driving field, while γ_m refers to the decay rate of the mechanical mode. In addition, we have used $a_{1,vac}$, $a_{2,vac}$, $a_{3,vac}$, and ξ to denote the input quantum noise operators with zero mean values $\langle a_{1,vac}\rangle = 0$, $\langle a_{2,vac}\rangle = 0$, $\langle a_{3,vac}\rangle = 0$, and $\langle\xi\rangle = 0$ [54].

Each operator of the optical and mechanical modes can be split into a classical mean value and a quantum fluctuation as usual. That means, we can set $a_j = \alpha_j + \delta a_j$, $a_{j,in} = \alpha_{j,in} + \delta a_{j,in}$, $q = \bar{q} + \delta q$, and $p = \bar{p} + \delta p$ with the ansatz $\alpha_j = \langle a_j\rangle$, $\alpha_{j,in} = \langle a_{j,in}\rangle$, $\bar{q} = \langle q\rangle$, and $\bar{p} = \langle p\rangle$. In the limit of a much stronger optical driving than the optomechanical coupling, that is, $\sqrt{\gamma_{j,e}}|\alpha_{j,in}| \gg \gamma_j \gg g$, the classical mean values and the fluctuation operators can be treated separately. Then we can determine the classical mean values, in the steady state ($\partial_t \alpha_i = \partial_t \bar{p} = \partial_t \bar{q} = 0$), via the following equations:

$$\begin{aligned} 0 &= -(\gamma_1/2 + i\Delta_1)\alpha_1 - ig\bar{q}\alpha_1 - iJ_{12}\alpha_2 + \sqrt{\gamma_{1,e}}\alpha_{1,in}, \\ 0 &= -(\gamma_2/2 + i\Delta_2)\alpha_2 - iJ_{12}\alpha_1 - iJ_{23}\alpha_3, \\ 0 &= -(\gamma_3/2 + i\Delta_3)\alpha_3 - iJ_{23}\alpha_2 + \sqrt{\gamma_{3,e}}\alpha_{3,in}, \\ 0 &= \bar{p}, \\ 0 &= -\omega_m\bar{q} - g|\alpha_1|^2, \end{aligned} \tag{3}$$

where the mean field approximation $\langle q\alpha_1\rangle \approx \langle q\rangle\langle\alpha_1\rangle$ has been taken into account. It is not difficult to see that the first (α_1) and third (α_3) optical modes are not reciprocal because the mean position $\bar{q}$ of the mechanical mode is just coupled to the mean amplitude α_1 of the first optical mode via $-ig\bar{q}\alpha_1$ with $\bar{q} = -g|\alpha_1|^2/\omega_m$. That means, the aforementioned equations do not remain unchanged if we exchange subscripts "1" and "3." Therefore, a transmission non-reciprocity is expected to occur no matter the driving field comes from either one direction ($\alpha_{1,in} \neq 0$ or $\alpha_{3,in} \neq 0$) or both directions ($\alpha_{1,in} \neq 0$ and $\alpha_{3,in} \neq 0$). With these classical mean values in hand, we can attain a set of linearized QLEs for the fluctuation operators in the matrix form

$$\frac{\partial f}{\partial t} = Af + \zeta, \tag{4}$$

by introducing two column vectors

$$\begin{aligned} f &= \left(\delta a_1, \delta a_1^\dagger, \delta a_2, \delta a_2^\dagger, \delta a_3, \delta a_3^\dagger, \delta q, \delta p\right)^T, \\ \zeta &= \left(\delta A_{1,in}, \delta A_{1,in}^\dagger, \delta A_{2,in}, \delta A_{2,in}^\dagger, \delta A_{3,in}, \delta A_{3,in}^\dagger, 0, \xi\right)^T \end{aligned} \tag{5}$$

and a coefficient matrix

$$A = \begin{bmatrix} -\left(\frac{\gamma_1}{2} + i\Delta_1'\right) & 0 & -iJ_{12} & 0 & 0 & 0 & -ig\alpha_1 & 0 \\ 0 & -\left(\frac{\gamma_1}{2} - i\Delta_1'\right) & 0 & iJ_{12} & 0 & 0 & ig\alpha_1^* & 0 \\ -iJ_{12} & 0 & -\left(\frac{\gamma_2}{2} + i\Delta_2\right) & 0 & -iJ_{23} & 0 & 0 & 0 \\ 0 & iJ_{12} & 0 & -\left(\frac{\gamma_2}{2} - i\Delta_2\right) & 0 & iJ_{23} & 0 & 0 \\ 0 & 0 & -iJ_{23} & 0 & -\left(\frac{\gamma_3}{2} + i\Delta_3\right) & 0 & 0 & 0 \\ 0 & 0 & 0 & iJ_{23} & 0 & -\left(\frac{\gamma_3}{2} - i\Delta_3\right) & 0 & 0 \\ 0 & 0 & 0 & 0 & 0 & 0 & 0 & \omega_m \\ -g\alpha_1^* & -g\alpha_1 & 0 & 0 & 0 & 0 & -\omega_m & -\gamma_m \end{bmatrix}, \tag{6}$$

where we have further defined $\delta A_{1,in} = \sqrt{\gamma_{1,e}}\delta a_{1,in} + \sqrt{\gamma_{1,i}}a_{1,vac}$, $\delta A_{2,in} = \sqrt{\gamma_{2,i}}a_{2,vac}$, $\delta A_{3,in} = \sqrt{\gamma_{3,e}}\delta a_{3,in} + \sqrt{\gamma_{3,i}}a_{3,vac}$, and $\Delta_1' = \Delta_1 + g\bar{q}$. Our optomechanical system can work in the stable regime only if all the eigenvalues of matrix A are negative in their real parts. This problem is difficult or impossible to be solved analytically but can be by numerically examined via the Routh–Hurwitz criterion [53] as adopted later.

In the following, we consider two specific cases where the driving field of amplitude $s_{in} = \sqrt{p_{in}/(\hbar\omega_d)}$ and power p_{in} is input just from the 1*st* optical mode with $\alpha_{1,in} = s_{in}$ and $\alpha_{3,in} = 0$ (*I*), or just from the 3*rd* optical mode with $\alpha_{1,in} = 0$ and $\alpha_{3,in} = s_{in}$ (*II*). In case (*I*), it is easy to attain from **Eq. 3** that

$$\begin{aligned} \alpha_3 &= \frac{-J_{12}J_{23}\alpha_1}{(\gamma_2/2 + i\Delta_2)(\gamma_3/2 + i\Delta_3) + J_{23}^2}, \\ \alpha_1 &= \frac{-J_{12}J_{23}\alpha_3 + (\gamma_2/2 + i\Delta_2)\sqrt{\gamma_{1,e}}s_{in}}{(\gamma_2/2 + i\Delta_2)(\gamma_1/2 + i\Delta_1 - iU|\alpha_1|^2) + J_{12}^2}, \end{aligned} \tag{7}$$

with $U = g^2/\omega_m$ characterizing the non-linear optomechanical interaction. Considering the input–output relation $\alpha_{3,out} = \sqrt{\gamma_{3,e}}\alpha_3$ [55, 56], we finally attain

$$\left(\Gamma/2 + i\bar{\Delta}\right)\alpha_{3,out} + iU_{31}|\alpha_{3,out}|^2\alpha_{3,out} = \varepsilon_{eff}. \tag{8}$$

In this equation, we have introduced the effective damping rate Γ, detuning $\bar{\Delta}$, non-linear interaction strength U_{31}, and driving amplitude ε_{eff} by setting

$$\begin{aligned} \Gamma &= \frac{A(\gamma_2\gamma_3/4 - \Delta_2\Delta_3 + J_{23}^2) + B(\gamma_2\Delta_3 + \gamma_3\Delta_2)}{|(\gamma_2/2 + i\Delta_2)(\gamma_3/2 + i\Delta_3) + J_{23}^2|^2}, \\ \bar{\Delta} &= \frac{B(\gamma_2\gamma_3/4 - \Delta_2\Delta_3 + J_{23}^2) - A(\gamma_2\Delta_3 + \gamma_3\Delta_2)/4}{|(\gamma_2/2 + i\Delta_2)(\gamma_3/2 + i\Delta_3) + J_{23}^2|^2}, \\ \varepsilon_{eff} &= \frac{-J_{12}J_{23}\sqrt{\gamma_{1,e}\gamma_{3,e}}s_{in}}{(\gamma_2/2 + i\Delta_2)(\gamma_3/2 + i\Delta_3) + J_{23}^2}, \\ U_{31} &= \frac{-U|(\gamma_2/2 + i\Delta_2)(\gamma_3/2 + i\Delta_3) + J_{23}^2|^2}{J_{12}^2J_{23}^2\gamma_{3,e}}, \end{aligned} \tag{9}$$

with newly defined coefficients

$$\begin{aligned} A &= \gamma_3(\gamma_1\gamma_2/4 - \Delta_1\Delta_2) - \Delta_3(\Delta_1\gamma_2 + \Delta_2\gamma_1) \\ &\quad + J_{23}^2\gamma_1 + J_{12}^2\gamma_3, \\ B &= \gamma_3(\Delta_1\gamma_2 + \Delta_2\gamma_1)/4 + \Delta_3(\gamma_1\gamma_2/4 - \Delta_1\Delta_2) \\ &\quad + J_{23}^2\Delta_1 + J_{12}^2\Delta_3. \end{aligned} \tag{10}$$

In case (*II*), we attain via a similar procedure.

$$\begin{aligned} \alpha_1 &= \frac{-J_{12}J_{23}\alpha_3}{(\gamma_1/2 + i\Delta_1 - iU|\alpha_1|^2)(\gamma_2/2 + i\Delta_2) + J_{12}^2}, \\ \alpha_3 &= \frac{-J_{12}J_{23}\alpha_1 + (\gamma_2/2 + i\Delta_2)\sqrt{\gamma_{3,e}}s_{in}}{(\gamma_2/2 + i\Delta_2)(\gamma_3/2 + i\Delta_3) + J_{23}^2}, \end{aligned} \tag{11}$$

which, when substituting into the input–output relation $\alpha_{1,out} = \sqrt{\gamma_{1,e}}\alpha_1$, finally yields

$$\left(\Gamma/2 + i\bar{\Delta}\right)\alpha_{1,out} + iU_{13}|\alpha_{1,out}|^2\alpha_{1,out} = \varepsilon_{eff}, \tag{12}$$

with a new effective non-linear interaction strength $U_{13} = -U/\gamma_{1,e}$, clearly different from U_{31}.

For convenience, we now translate **Eqs 8, 12** into a unified form in terms of $X_i = |\alpha_{i,out}|^2$

$$\left(\Gamma^2/4 + \bar{\Delta}^2\right)X_i + 2\bar{\Delta}U_{eff}X_i^2 + U_{eff}^2X_i^3 = |\varepsilon_{eff}|^2, \tag{13}$$

with $U_{eff} = U_{13}$ for $X_1 = |\alpha_{1,out}|^2$, while $U_{eff} = U_{31}$ for $X_3 = |\alpha_{3,out}|^2$. This non-linear equation indicates that X_i can take three real values, corresponding to the bistability of output against input, under appropriate conditions. One way for determining the bistable region is to take a derivative of **Eq. 13** with respect to X_i, yielding

$$\left(\Gamma^2/4 + \bar{\Delta}^2\right) + 4\bar{\Delta}U_{eff}X_i + 3U_{eff}^2X_i^2 = 0, \tag{14}$$

whose two positive roots

$$X_i^\pm = \frac{-4\bar{\Delta} \mp \sqrt{4\bar{\Delta}^2 - 3\Gamma^2}}{6U_{eff}} > 0, \tag{15}$$

restricted by $\bar{\Delta} < -\sqrt{3}\Gamma/2$ referring to two turning points of the bistable region. That means, the solution of **Eq. 15** takes three branches in the bistable region of $X_i^- \leq X_i \leq X_i^+$. The intermediate branch is known to be definitely unstable because it corresponds to the maximum (not minimum) point in an effective potential, while the upper and lower branches are usually stable, for example, in a non-linear Kerr medium [57, 58]. In our optomechanical system, the upper branch may also be unstable as the mechanical mode exhibits a negative effective damping rate owing to a heating effect in the blue-detuned or strong-driving regime, which will be numerically examined via the Routh–Hurwitz criterion [53].

The expected non-linear bistability is straightforward to be examined by two transmission coefficients:

$$\begin{aligned} T_{31} &= |\alpha_{3,out}/\alpha_{1,in}|^2, \\ T_{13} &= |\alpha_{1,out}/\alpha_{3,in}|^2, \end{aligned} \tag{16}$$

referring, respectively, to a transport from the $1st$ optical mode to the $3rd$ optical mode and that from the $3rd$ optical mode to the $1st$ optical mode. Considering that U_{31} and U_{13} have different expressions, we know from **Eqs 8, 12** that $a_{3,out} \neq a_{1,out}$ in general and therefore $T_{31} \neq T_{13}$ for light signals of amplitudes $a_{1,in} = a_{2,in} = s_{in}$ input from the opposite sides of our optomechanical system. The efficiency of such a non-reciprocal transport can be quantified by defining

$$I_{tr} = 10\log(T_{31}/T_{13}), \tag{17}$$

as the isolation ratio. We should note however that it is also possible to have $U_{31} = U_{13}$ in the case of

$$\gamma_{1,e} = \frac{J_{12}^2 J_{23}^2 \gamma_{3,e}}{|(\gamma_2/2 + i\Delta_2)(\gamma_3/2 + i\Delta_3) + J_{23}^2|^2}, \tag{18}$$

referred to as the impedance-matching condition, from which it is viable to get a critical coupling strength

$$J_{23}^c = \sqrt{\frac{\gamma_{3,e}J_{12}^2 - 2\gamma_{1,e}(\gamma_2\gamma_3/4 - \Delta_2\Delta_3) \pm \sqrt{C}}{2\gamma_{1,e}}}, \tag{19}$$

with $C = \gamma_{3,e}^2 J_{12}^4 - \gamma_{1,e}\gamma_{3,e}J_{12}^2(\gamma_2\gamma_3 - 4\Delta_2\Delta_3) - \gamma_{1,e}^2(\gamma_2\Delta_3 - \Delta_2\gamma_3)$ independent of input power p_{in}. It is clear that in the case of $J_{23} \neq J_{23}^c$, the impedance-matching condition will be broken, and we could have unequal (optomechanical) non-linear interaction strengths $U_{31} \neq U_{13}$. This would result in the optical transmission non-reciprocity characterized by $T_{31} \neq T_{13}$ and thus $I_{tran} \neq 0$.

3 RESULTS AND DISCUSSION

In this section, we examine the effects of relevant tunable parameters on the non-reciprocal bistable transmission of light signals input from the opposite sides of our optomechanical system via numerical calculations. Most parameters are chosen based on two recent works and accessible in up-to-date experiments [31, 44], among which $\gamma_1/2\pi = 1.0$ GHz, $\gamma_2/2\pi = 0.5$ GHz, $\gamma_3/2\pi = 4.5$ GHz, $\eta_1 = \eta_2 = \eta_3 = 0.9$, $\omega_d/2\pi = 300$ THz, and $\gamma_m/2\pi = 6.0$ MHz are fixed in the following discussions. Numerical results will be shown in two cases where transmission coefficients T_{31} and T_{13} are plotted against input power p_{in} and detuning Δ_1, respectively, as they are much easier to modulate in regard of real applications. The main difficulty relevant to an experimental realization of our proposal lies in that the accurate preparation and arrangement of three (micro)coupled cavities of identical optical modes while different decay rates. A (micro) mechanical oscillator of proper resonant frequency and optomechanical coupling strength may also be hard to be integrated with one (micro)optical cavity.

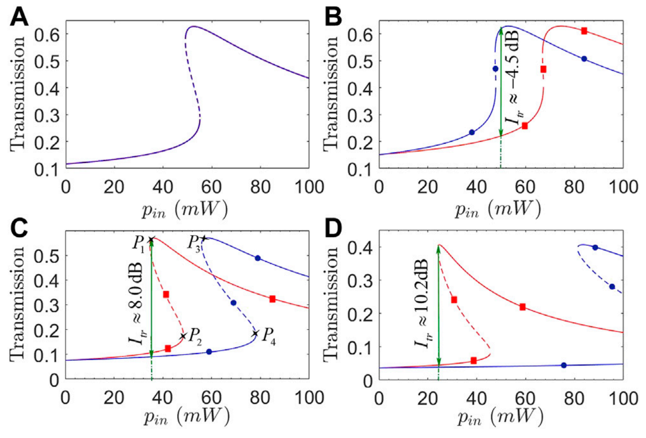

FIGURE 2 | (Color online) Transmission coefficients T_{31} (red squares) and T_{13} (blue circles) against input power p_{in} with **(A)** $J_{23}/2\pi = 1.725$ GHz; **(B)** $J_{23}/2\pi = 2.0$ GHz; **(C)** $J_{23}/2\pi = 1.4$ GHz; **(D)** $J_{23}/2\pi = 1.0$ GHz. Solid and dashed parts of each curve refer to stable and unstable regions, respectively. Other parameters are $\Delta_1/2\pi = \Delta_2/2\pi = 4.5$ GHz, $\Delta_3/2\pi = 1.5$ GHz, $g/2\pi = 0.9$ MHz, $\omega_m/2\pi = 10$ GHz, and $J_{12}/2\pi = 3.0$ GHz, except those at the beginning of **Section 3**.

3.1 Non-Reciprocal Transmission Against Input Power

In **Figure 2**, we plot transmission coefficients T_{31} and T_{13} as a function of input power p_{in} for different optical coupling strengths J_{23}. **Figure 2A** shows that transmission non-reciprocity (i.e., $T_{13} \neq T_{31}$ or $I_{tran} \neq 0$) cannot be attained as the impedance-matching condition is well satisfied with $J_{23}/2\pi = J_{23}^c/2\pi \simeq 1.725$ GHz, though our optomechanical system works in the bistable regime. Increasing or decreasing J_{23} to deviate from the critical value J_{23}^c, we can see from **Figures 2B–D** that transmission non-reciprocity occurs with different isolation ratios for different input powers. We have, in particular, that $I_{tr} \approx -4.5$ dB for $p_{in} = 50$ mW in the case of $J_{23}/2\pi = 2.0$ GHz, $I_{tr} \approx 8.0$ dB for $p_{in} = 36$ mW in the case of $J_{23}/2\pi = 1.4$ GHz, and $I_{tr} \approx 10.2$ dB for $p_{in} = 25$ mW in the case of $J_{23}/2\pi = 1.0$ GHz. These results indicate that it is viable to reverse the transmission non-reciprocity from $I_{tr} < 0$ to $I_{tr} > 0$ ($I_{tr} > 0$ to $I_{tr} < 0$) as J_{23} is decreased (increased) to cross the critical value J_{23}^c, and we can attain higher isolation ratios in wider bistable regions by modulating J_{23} to be more deviating from the critical value J_{23}^c. Taking **Figure 2C** as an example, it is also important to note that we should choose to work in the region between turning points P_2 and P_4 as p_{in} is increased from a small value, while between P_1 and P_3 as p_{in} is decreased from a large value. This promises for attaining a more efficient transmission non-reciprocity corresponding to a larger $|I_{tr}|$ because it can be evaluated with the upper branch of T_{31} and the lower branch of T_{13}. Otherwise, T_{31} and T_{13} will both work in the lower or

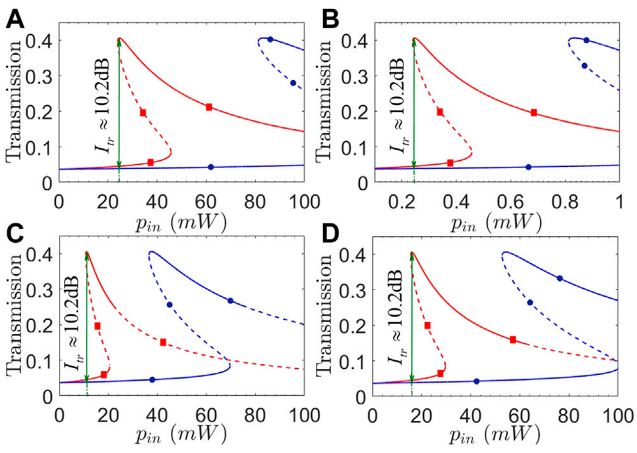

FIGURE 3 | (Color online) Transmission coefficients T_{31} (red squares) and T_{13} (blue circles) against input power p_{in} with **(A)** $g/2\pi = 0.9$ MHz; **(B)** $g/2\pi = 9.0$ MHz; **(C)** $\omega_m/2\pi = 4.5$ GHz; **(D)** $\omega_m/2\pi = 6.5$ GHz. Solid and dashed parts of each curve refer to stable and unstable regions, respectively. Other parameters are the same as in **Figure 2**, except $J_{23}/2\pi = 1.0$ GHz.

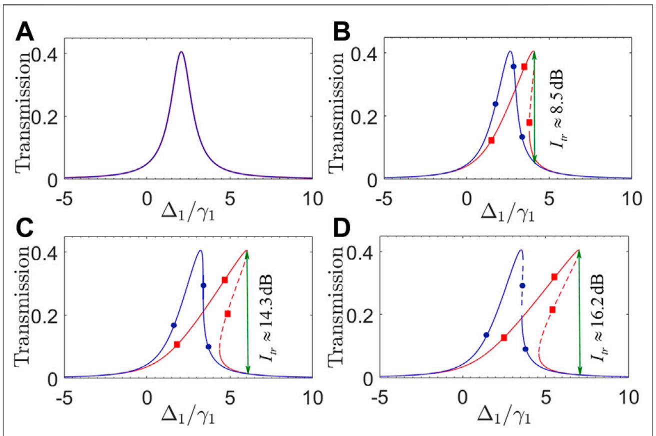

FIGURE 5 | (Color online) Transmission coefficients T_{31} (red squares) and T_{13} (blue circles) against detuning Δ_1 with **(A)** $p_{in} = 0.1$ mW; **(B)** $p_{in} = 20$ mW; **(C)** $p_{in} = 40$ mW; **(D)** $p_{in} = 50$ mW. Solid and dashed parts of each curve refer to stable and unstable regions, respectively. Other parameters are $\Delta_2/2\pi = 4.5$ GHz, $\Delta_3/2\pi = 1.5$ GHz, $g/2\pi = 0.9$ MHz, $\omega_m/2\pi = 10$ GHz, $J_{12}/2\pi = 3.0$ GHz, and $J_{23} = 1.0$ GHz, except those at the beginning of **Section 3**.

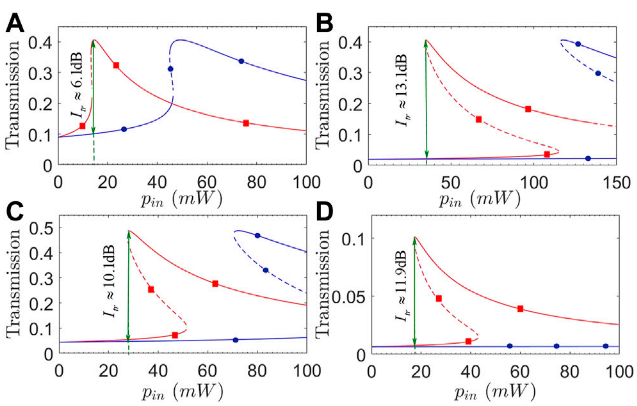

FIGURE 4 | (Color online) Transmission coefficients T_{31} (red squares) and T_{13} (blue circles) against input power p_{in} with **(A)** $\Delta_1/2\pi = 3.5$ GHz; **(B)** $\Delta_1/2\pi = 5.5$ GHz; **(C)** $\Delta_3/2\pi = 0.1$ GHz; **(D)** $\Delta_3/2\pi = 6.0$ GHz. Solid and dashed parts of each curve refer to stable and unstable regions, respectively. Other parameters are the same as in **Figure 2**, except $J_{23}/2\pi = 1.0$ GHz.

upper branch to result in well suppressed transmission non-reciprocity of smaller or vanishing $|I_{tr}|$.

Comparing **Eqs 8**, **12**, it is easy to see that the transmission non-reciprocity will be attained as long as we have $U_{13} \neq U_{31}$, which requires not only a broken impedance-matching condition but also $U = g^2/\omega_m \neq 0$. Thus, it is essential to examine in **Figure 3** different effects of optomechanical coupling strength g and mechanical frequency ω_m on transmission coefficients T_{31} and T_{13} plotted against input power p_{in}. **Figures 3A,B** show that as g is enhanced by one order, p_{in} required for observing the transmission non-reciprocity (in the bistable region where T_{13} and T_{31} work in the lower and upper branches, respectively) is reduced by two orders without changing the maximal isolation ratio $I_{tr} \approx 10.2$ dB. That means the observed transmission non-reciprocity exhibits an inverse dependence on input power p_{in} and optomechanical coupling strength g. **Figures 3C,D** further show that the non-reciprocal region in terms of p_{in} is not so sensitive to ω_m though this region can be enlarged in the case of a larger ω_m. It is more important to note that the upper branches of T_{31} and T_{13} may not be always stable and a larger ω_m is helpful to reduce the unstable regions. These findings tell us how to choose g and ω_m for attaining a wide enough non-reciprocal region corresponding to low enough input powers.

Considering that the driving field and relevant optical modes are easy to be modulated in frequency, we plot in **Figure 4** transmission coefficients T_{31} and T_{13} as a function of input power p_{in} for different detunings Δ_1 and Δ_3. We can see from **Figures 4A,B** that the isolation ratio may be evidently improved in a wider non-reciprocal region by choosing a slightly larger Δ_1 to well suppress the lower branches of T_{31} and T_{13}, while leaving the upper branches unchanged yet in magnitude. To be more specific, we have $I_{tr} \approx 6.1$ dB for $p_{in} = 14$ mW with $\Delta_1/2\pi = 3.5$ GHz, while $I_{tr} \approx 13.1$ dB for $p_{in} = 35$ mW with $\Delta_1/2\pi = 5.5$ GHz. **Figures 4C,D** show instead that a significant increase of Δ_3, though can result in a wider non-reciprocal region, will not change the isolation ratio too much as the upper and lower branches are suppressed to the roughly same extent. We also note from **Figure 4B** that the upper branch of T_{31} starts to become unstable at $p_{in} \gtrsim 140$ mW for $\Delta_1 = 5.5$ GHz. It is thus clear that detunings Δ_1 and Δ_3 play different roles in manipulating the transmission non-reciprocity and can be jointly modulated for observing an ideal transmission non-reciprocity with larger isolation ratios and well suppressed lower branches for moderate input powers.

3.2 Non-Reciprocal Transmission Against Detuning

We first plot in **Figure 5** transmission coefficients T_{31} and T_{13} as a function of detuning Δ_1 for different input powers p_{in}. As the

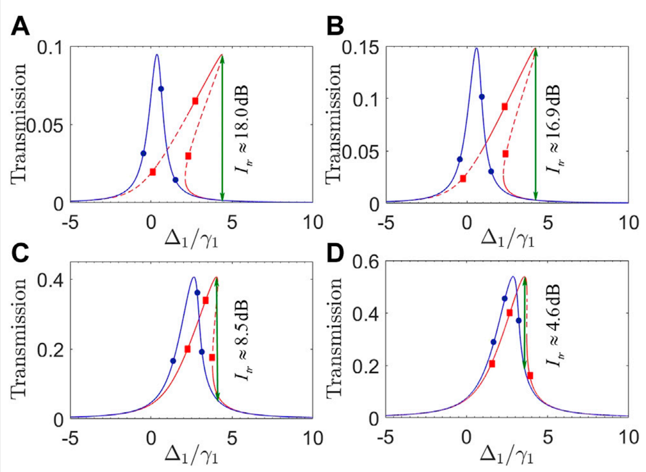

FIGURE 6 | (Color online) Transmission coefficients T_{31} (red squares) and T_{13} (blue circles) against detuning Δ_1 with **(A)** $J_{12}/2\pi = 1.0$ GHz; **(B)** $J_{12}/2\pi = 1.3$ GHz; **(C)** $J_{23}/2\pi = 1.0$ GHz; **(D)** $J_{23}/2\pi = 1.3$ GHz. Solid and dashed parts of each curve refer to stable and unstable regions, respectively. Other parameters are the same as in **Figure 5**, except $p_{in} = 20$ mW.

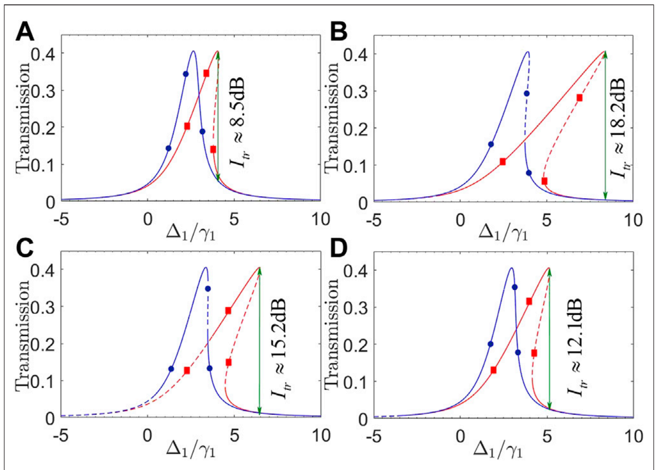

FIGURE 7 | (Color online) Transmission coefficients T_{31} (red squares) and T_{13} (blue circles) against detuning Δ_1 with **(A)** $g/2\pi = 0.9$ MHz; **(B)** $g/2\pi = 1.6$ MHz; **(C)** $\omega_m/2\pi = 4.5$ GHz; **(D)** $\omega_m/2\pi = 6.5$ GHz. Solid and dashed parts of each curve refer to stable and unstable regions, respectively. Other parameters are the same as in **Figure 5**, except $p_{in} = 20$ mW.

input power is very low (i.e., $p_{in} = 0.1$ mW), **Figure 5A** shows that T_{31} and T_{13} overlap well with a symmetric peak centered at $\Delta_1 \approx (J_{12} + J_{23})/2 = 2$ GHz, therefore leading to a vanishing transmission non-reciprocity. This can be attributed to the fact that both **Eqs 8, 12** reduce to $(\Gamma/2 + i\bar{\Delta})\alpha_{j,out} \approx \varepsilon_{eff}$ when $U_{jj'}|\alpha_{j,out}|^2$ with $j + j' = 4$ is much smaller than $\bar{\Delta}$. As the input power increases to be large enough, we find from **Figures 5B–D** that T_{31} and T_{13} start to exhibit different bistable behaviors and thus become distinguishable on the side of $\Delta_1 > (J_{12} + J_{23})/2$ because U_{13} and U_{31} always take negative values. That means the deviation of a transmission peak from its original position may serve as a good estimation on the strength of non-linear optomechanical interaction. To be more specific, the input power p_{in} has less influence on T_{13} than T_{31} so that the transmission non-reciprocity occurs and becomes more and more evident as p_{in} increases. It is also noted that a larger input power always results in a wider bistable region with a higher isolation ratio at the right turning point of T_{31}: $I_{tr} \approx 8.5$ dB at $\Delta_1/\gamma_1 = 4.0$ for $p_{in} = 20$ mW; $I_{tr} \approx 14.3$ dB at $\Delta_1/\gamma_1 = 6.0$ for $p_{in} = 40$ mW; $I_{tr} \approx 16.2$ dB at $\Delta_1/\gamma_1 = 7.0$ for $p_{in} = 50$ mW.

Then we examine different effects of optical coupling strengths J_{12} and J_{23} by plotting in **Figure 6** transmission coefficients T_{31} and T_{13} against detuning Δ_1. **Figures 6A,B** show that a slight increase in J_{12} will result in an evidently identical rising of T_{31} and T_{13} but leaving their peaks roughly unchanged in position. The main difference lies in that the upper branch of T_{31} in **Figure 6A** exhibits a wider stable region than that in **Figure 6B**, indicating that a larger J_{12} helps to suppress quantum fluctuations arising from the non-linear optomechanical interaction. On the other hand, **Figures 6C,D** show that a slight increase in J_{23} can also result in an evidently identical rising of T_{31} and T_{13}, but their peaks become evidently closer to each other, leading to a narrowing of the non-reciprocal bistable region as well as a reduction in the isolation ratio. These findings tell that a moderate J_{23} and a larger J_{12} are appropriate for attaining non-reciprocal bistable regions of wide enough stable upper branches and large enough isolation ratios.

Finally, we examine different effects of mechanical frequency ω_m and optomechanical coupling strength g by plotting in **Figure 7** transmission coefficients T_{31} and T_{13} against detuning Δ_1. Comparing **Figures 7A,B**, we can see that both T_{31} and T_{13} remain unchanged in their peak values but clearly become more inclined toward $\Delta_1 > 0$ so as to yield wider bistable regions, with the increase in g. This then results in a wider non-reciprocal transmission region considering that T_{31} is much more sensitive to g and thus exhibits a much wider bistable region than T_{13}. **Figures 7C,D** show however that an increase in ω_m is helpful to reduce the unstable region of T_{31} in its upper branch but meanwhile also results in a reduction of the bistable regions for both T_{31} and T_{13}. These findings tell that one should choose a lower ω_m and a higher g to enhance the non-linear optomechanical interaction required for attaining wider non-reciprocal transmission regions of high isolation ratios.

In figures, the bistable transmission non-reciprocity occurs as the two curves for T_{31} and T_{13} do not overlap in each plot. It is thus appropriate to roughly determine a non-reciprocal bandwidth as the absolute difference of two values of p_{in} or Δ_1 corresponding, respectively, to the peak of T_{31} and that of T_{13}. This non-reciprocal bandwidth is a few or tens of mW in **Figures 2–4**, while several times of γ_1 in **Figures 5–7**, depending on relevant parameters like J_{12}, J_{23}, g, and ω_m. Note also that a dynamic reciprocity, referring to the fact that a (weak) backward noise, can also be transmitted with little loss in the presence of a (strong) forward signal of high transmission, typically exists in the non-reciprocal systems based on optical non-linearities [59].

Accordingly, one limitation of our optomechanical system may be that it cannot break the dynamic reciprocity because the transmission non-reciprocity arises from a bistable non-linearity. This is clear by looking at **Figures 2–4** where we have $T_{31} \neq T_{13}$ only when input power p_{in} is not too small.

4 CONCLUSION

In summary, we have studied a four-mode optomechanical system for attaining the transmission non-reciprocity, in the presence of an optomechanically induced non-linearity, with respect to a driving field input from the left or right side. As the impedance-matching condition is broken, we find that transmission coefficients T_{31} and T_{13}, plotted against input power p_{in} or cavity detuning Δ_1, may exhibit staggered bistable behaviors and therefore can work in the upper and lower branches, respectively. The isolation ratio of such a non-reciprocal transmission is viable to switch between $I_{tr} > 0$ and $I_{tr} < 0$ and can be improved in magnitude by modulating optical coupling strengths $J_{12,23}$ and detunings $\Delta_{1,3}$ to suppress the lower branches or enhance the upper branches. It is also viable to broaden the non-reciprocal bistable region in terms of p_{in} (Δ_1) by modulating optomechanical coupling strength g and mechanical frequency ω_m in addition to $J_{12,23}$ and $\Delta_{1,3}$ (p_{in}). But we should note that an increasing part of the upper branch may become unstable as the non-reciprocal region becomes wider, which restricts the tunable ranges of relevant parameters. Our results well extend the previous works on realizing non-reciprocal transmission in optomechanical systems and are instructive for designing non-reciprocal devices in optical networks based on coupled cavities.

DATA AVAILABILITY STATEMENT

The original contributions presented in the study are included in the article/supplementary material; further inquiries can be directed to the corresponding authors.

AUTHOR CONTRIBUTIONS

The idea was first conceived by J-HW. BJ was responsible for the physical modeling, the numerical calculations, and writing most of the manuscript. J-HW contributed to writing the manuscript, JW verified results of the theoretical calculation, and DY contributed to the discussion of the results. DQ provided technical support in computer simulation.

FUNDING

This work is supported by the National Natural Science Foundation of China (12074061, 11674049, and 11874004), Science Foundation of Education Department of Jilin Province (JJKH20200557KJ), and Nature Science Foundation of Science and Technology Department of Jilin Province (20210101411JC).

ACKNOWLEDGMENTS

BJ thanks Luning Song, Yan Zhang, and Zhihai Wang for helpful discussions.

REFERENCES

1. Teufel JD, Harlow JW, Regal CA, Lehnert KW. Dynamical Backaction of Microwave fields on a Nanomechanical Oscillator. *Phys Rev Lett* (2008) 101: 197203. doi:10.1103/PhysRevLett.101.197203
2. Aspelmeyer M, Kippenberg TJ, Marquardt F. Cavity Optomechanics. *Rev Mod Phys* (2014) 86:1391–452. doi:10.1103/RevModPhys.86.1391
3. Liu Y-C, Hu Y-W, Wong C-W, Xiao Y-F. Review of Cavity Optomechanical Cooling. *Chin Phys B* (2013) 22:114213. doi:10.1088/1674-1056/22/11/114213
4. He B. Quantum Optomechanics beyond Linearization. *Phys Rev A* (2012) 85: 063820. doi:10.1103/PhysRevA.85.063820
5. Cao C, Mi S-C, Gao Y-P, He L-Y, Yang D, Wang T-J, et al. Tunable High-Order Sideband Spectra Generation Using a Photonic Molecule Optomechanical System. *Sci Rep* (2016) 6:1–8. doi:10.1038/srep22920
6. Xiong X-R, Gao Y-P, Liu X-F, Cao C, Wang T-J, Wang C. The Analysis of High-Order Sideband Signals in Optomechanical System. *Sci China Phys Mech Astron* (2018) 61:1–4. doi:10.1007/s11433-017-9187-2
7. Shi H-Q, Xie Z-Q, Xu X-W, Liu N-H. Unconventional Phonon Blockade in Multimode Optomechanical System. *Acta Phys Sin* (2018) 67:044203. doi:10.7498/aps.67.20171599
8. Marinković I, Wallucks A, Riedinger R, Hong S, Aspelmeyer M, Gröblacher S. Optomechanical bell Test. *Phys Rev Lett* (2018) 121:220404. doi:10.1103/PhysRevLett.121.220404
9. Xu H, Lai D-G, Qian Y-B, Hou B-P, Miranowicz A, Nori F. Optomechanical Dynamics in the PT - and Broken- PT -symmetric regimes*mathcalPT*- and broken-*mathcalPT*-symmetric Regimes. *Phys Rev A* (2021) 104:053518. doi:10.1103/PhysRevA.104.053518
10. Vitali D, Gigan S, Ferreira A, Böhm HR, Tombesi P, Guerreiro A, et al. Optomechanical Entanglement between a Movable Mirror and a Cavity Field. *Phys Rev Lett* (2007) 98:030405. doi:10.1103/PhysRevLett.98.030405
11. Chen R-X, Shen L-T, Yang Z-B, Wu H-Z, Zheng S-B. Enhancement of Entanglement in Distant Mechanical Vibrations via Modulation in a Coupled Optomechanical System. *Phys Rev A* (2014) 89:023843. doi:10.1103/PhysRevA.89.023843
12. Liao J-Q, Wu Q-Q, Nori F. Entangling Two Macroscopic Mechanical Mirrors in a Two-Cavity Optomechanical System. *Phys Rev A* (2014) 89:014302. doi:10.1103/PhysRevA.89.014302
13. Yan X-B. Enhanced Output Entanglement with Reservoir Engineering. *Phys Rev A* (2017) 96:053831. doi:10.1103/PhysRevA.96.053831
14. He Q, Ficek Z. Einstein-podolsky-rosen Paradox and Quantum Steering in a Three-Mode Optomechanical System. *Phys Rev A* (2014) 89:022332. doi:10.1103/PhysRevA.89.022332
15. Zhang X-L, Bao Q-Q, Yang M-Z, Tian X-S. Entanglement Characteristics of Output Optical fields in Double-Cavity Optomechanics. *Acta Phys Sin* (2018) 67:104203. doi:10.7498/aps.67.20172467
16. Poot M, Herre SJ. Mechanical Systems in the Quantum Regime. *Phys Rep* (2012) 511:273–335. doi:10.1016/j.physrep.2011.12.004
17. He B, Yang L, Lin Q, Xiao M. Radiation Pressure Cooling as a Quantum Dynamical Process. *Phys Rev Lett* (2017) 118:233604. doi:10.1103/PhysRevLett.118.233604
18. Chen H-J, Mi X-W. Normal Mode Splitting and Cooling in strong Coupling Optomechanical Cavity. *Acta Phys Sin* (2011) 60:124206–244. doi:10.7498/aps.60.124206
19. Li Y, Wu L-A, Wang Z-D. Fast Ground-State Cooling of Mechanical Resonators with Time-dependent Optical Cavities. *Phys Rev A* (2011) 83: 043804. doi:10.1103/PhysRevA.83.043804

20. Liu Z-Q, Hu C-S, Jiang Y-K, Su W-J, Wu H, Li Y, et al. Engineering Optomechanical Entanglement via Dual-Mode Cooling with a Single Reservoir. *Phys Rev A* (2021) 103:023525. doi:10.1103/PhysRevA.103.023525
21. Bai C, Hou B-P, Lai D-G, Wu D. Tunable Optomechanically Induced Transparency in Double Quadratically Coupled Optomechanical Cavities within a Common Reservoir. *Phys Rev A* (2016) 93:043804. doi:10.1103/PhysRevA.93.043804
22. Yan X-B. Optomechanically Induced Transparency and Gain. *Phys Rev A* (2020) 101:043820. doi:10.1103/PhysRevA.101.043820
23. Lü H, Wang C, Yang L, Jing H. Optomechanically Induced Transparency at Exceptional Points. *Phys Rev Appl* (2018) 10:014006. doi:10.1103/PhysRevApplied.10.014006
24. Hou B-P, Wei L-F, Wang S-J. Optomechanically Induced Transparency and Absorption in Hybridized Optomechanical Systems. *Phys Rev A* (2015) 92:033829. doi:10.1103/PhysRevA.92.033829
25. Qu K, Agarwal GS. Phonon-mediated Electromagnetically Induced Absorption in Hybrid Opto-Electromechanical Systems. *Phys Rev A* (2013) 87:031802. doi:10.1103/PhysRevA.87.031802
26. Zhang J-Q, Li Y, Feng M, Xu Y. Precision Measurement of Electrical Charge with Optomechanically Induced Transparency. *Phys Rev A* (2012) 86:053806. doi:10.1103/PhysRevA.86.053806
27. Brunner N, Cavalcanti D, Pironio S, Scarani V, Wehner S. Bell Nonlocality. *Rev Mod Phys* (2014) 86:419–78. doi:10.1103/RevModPhys.86.419
28. Lü X-Y, Jing H, Ma J-Y, Wu Y. PT-Symmetry-Breaking Chaos in Optomechanics. *Phys Rev Lett* (2015) 114:253601. doi:10.1103/PhysRevLett.114.253601
29. Margueritat J, Virgone-Carlotta A, Monnier S, Delanoë-Ayari H, Mertani HC, Berthelot A, et al. High-frequency Mechanical Properties of Tumors Measured by Brillouin Light Scattering. *Phys Rev Lett* (2019) 122:018101. doi:10.1103/PhysRevLett.122.018101
30. Song L-N, Zheng Q, Xu X-W, Jiang C, Li Y. Optimal Unidirectional Amplification Induced by Optical Gain in Optomechanical Systems. *Phys Rev A* (2019) 100:043835. doi:10.1103/PhysRevA.100.043835
31. Xu X-W, Song L-N, Zheng Q, Wang Z-H, Li Y. Optomechanically Induced Nonreciprocity in a Three-Mode Optomechanical System. *Acta Phys Sin* (2018) 98:063845. doi:10.1103/PhysRevA.98.063845
32. Zhang L-W, Li X-L, Yang L. Optical Nonreciprocity with Blue-Detuned Driving in Two-Cavity Optomechanics. *Acta Phys Sin* (2019) 68:170701–9. doi:10.7498/aps.68.20190205
33. Miri M-A, Ruesink F, Verhagen E, Alù A. Optical Nonreciprocity Based on Optomechanical Coupling. *Phys Rev Appl* (2017) 7:064014. doi:10.1103/PhysRevApplied.7.064014
34. Li E-Z, Ding D-S, Yu Y-C, Dong M-X, Zeng L, Zhang W-H, et al. Experimental Demonstration of Cavity-free Optical Isolators and Optical Circulators. *Phys Rev Res* (2020) 2:033517. doi:10.1103/PhysRevResearch.2.033517
35. Li B, Özdemir ŞK, Xu X-W, Zhang L, Kuang L-M, Jing H. Nonreciprocal Optical Solitons in a Spinning Kerr Resonator. *Phys Rev A* (2021) 103:053522. doi:10.1103/PhysRevA.103.053522
36. Verhagen E, Alù A. Optomechanical Nonreciprocity. *Nat Phys* (2017) 13:922–4. doi:10.1038/nphys4283
37. Lira H, Yu Z, Fan S, Lipson M. Electrically Driven Nonreciprocity Induced by Interband Photonic Transition on a Silicon Chip. *Phys Rev Lett* (2012) 109:033901. doi:10.1103/PhysRevLett.109.033901
38. Manipatruni S, Robinson JT, Lipson M. Optical Nonreciprocity in Optomechanical Structures. *Phys Rev Lett* (2009) 102:213903. doi:10.1103/PhysRevLett.102.213903
39. Gridnev VN. Nonreciprocal Reflection of Light from Antiferromagnets. *Jetp Lett* (1996) 64:110–3. doi:10.1134/1.567141
40. Lu X, Cao W, Yi W, Shen H, Xiao Y. Nonreciprocity and Quantum Correlations of Light Transport in Hot Atoms via Reservoir Engineering. *Phys Rev Lett* (2021) 126:223603. doi:10.1103/PhysRevLett.126.223603
41. Wang Y-P, Rao J-W, Yang Y, Xu P-C, Gui Y-S, Yao B-M, et al. Nonreciprocity and Unidirectional Invisibility in Cavity Magnonics. *Phys Rev Lett* (2019) 123:127202. doi:10.1103/PhysRevLett.123.127202
42. Lai D-G, Huang J-F, Yin X-L, Hou B-P, Li W, Vitali D, et al. Nonreciprocal Ground-State Cooling of Multiple Mechanical Resonators. *Phys Rev A* (2020) 102:011502. doi:10.1103/PhysRevA.102.011502
43. Khanikaev AB, Mousavi SH, Shvets G, Kivshar YS. One-way Extraordinary Optical Transmission and Nonreciprocal Spoof Plasmons. *Phys Rev Lett* (2010) 105:126804. doi:10.1103/PhysRevLett.105.126804
44. Fang K, Luo J, Metelmann A, Matheny MH, Marquardt F, Clerk AA, et al. Generalized Non-reciprocity in an Optomechanical Circuit via Synthetic Magnetism and Reservoir Engineering. *Nat Phys* (2017) 13:465–71. doi:10.1038/nphys4009
45. Dzyaloshinskii I, Papamichail EV. Nonreciprocal Optical Rotation in Antiferromagnets. *Phys Rev Lett* (1995) 75:3004–7. doi:10.1103/PhysRevLett.75.3004
46. Ni X, He C, Sun X-C, Liu X-P, Lu M-H, Feng L, et al. Topologically Protected One-Way Edge Mode in Networks of Acoustic Resonators with Circulating Air Flow. *New J Phys* (2015) 17:053016. doi:10.1088/1367-2630/17/5/053016
47. Yu H, Wang Z, Wu J-H. Entanglement Preparation and Nonreciprocal Excitation Evolution in Giant Atoms by Controllable Dissipation and Coupling. *Phys Rev A* (2021) 104:013720. doi:10.1103/PhysRevA.104.013720
48. Du L, Cai M-R, Wu J-H, Wang Z, Li Y. Single-photon Nonreciprocal Excitation Transfer with Non-markovian Retarded Effects. *Phys Rev A* (2021) 103:053701. doi:10.1103/PhysRevA.103.053701
49. Zhang S, Hu Y, Lin G, Niu Y, Xia K, Gong J, et al. Thermal-motion-induced Non-reciprocal Quantum Optical System. *Nat Photon* (2018) 12:744–8. doi:10.1038/s41566-018-0269-2
50. Xia K, Nori F, Min X. Cavity-free Optical Isolators and Circulators Using a Chiral Cross-Kerr Nonlinearity. *Phys Rev Lett* (2018) 121:203602. doi:10.1103/PhysRevLett.121.203602
51. Hu Y, Zhang S, Qi Y, Lin G, Niu Y, Gong S. Multiwavelength Magnetic-free Optical Isolator by Optical Pumping in Warm Atoms. *Phys Rev Appl* (2019) 12:054004. doi:10.1103/PhysRevApplied.12.054004
52. Paraïso TK, Kalaee M, Zang L, Pfeifer H, Marquardt F, Painter O. Position-squared Coupling in a Tunable Photonic crystal Optomechanical Cavity. *Phys Rev X* (2015) 5:041024. doi:10.1103/PhysRevX.5.041024
53. DeJesus EX, Kaufman C. Routh-hurwitz Criterion in the Examination of Eigenvalues of a System of Nonlinear Ordinary Differential Equations. *Phys Rev A* (1987) 35:5288–90. doi:10.1103/PhysRevA.35.5288
54. Paternostro M, Gigan S, Kim MS, Blaser F, Böhm HR, Aspelmeyer M. Reconstructing the Dynamics of a Movable Mirror in a Detuned Optical Cavity. *New J Phys* (2006) 8:107. doi:10.1088/1367-2630/8/6/107
55. Gardiner CW, Collett MJ. Input and Output in Damped Quantum Systems: Quantum Stochastic Differential Equations and the Master Equation. *Phys Rev A* (1985) 31:3761–74. doi:10.1103/PhysRevA.31.3761
56. Agarwal GS, Huang S. Optomechanical Systems as Single-Photon Routers. *Phys Rev A* (2012) 85:021801. doi:10.1103/PhysRevA.85.021801
57. Aldana S, Bruder C, Nunnenkamp A. Equivalence between an Optomechanical System and a Kerr Medium. *Phys Rev A* (2013) 88:043826. doi:10.1103/PhysRevA.88.043826
58. Fabre C, Pinard M, Bourzeix S, Heidmann A, Giacobino E, Reynaud S. Quantum-noise Reduction Using a Cavity with a Movable Mirror. *Phys Rev A* (1994) 49:1337–43. doi:10.1103/PhysRevA.49.1337
59. Shi Y, Yu Z, Fan S. Limitations of Nonlinear Optical Isolators Due to Dynamic Reciprocity. *Nat Photon* (2015) 9:388–92. doi:10.1038/nphoton.2015.79

Conflict of Interest: The authors declare that the research was conducted in the absence of any commercial or financial relationships that could be construed as a potential conflict of interest.

Publisher's Note: All claims expressed in this article are solely those of the authors and do not necessarily represent those of their affiliated organizations, or those of the publisher, the editors, and the reviewers. Any product that may be evaluated in this article, or claim that may be made by its manufacturer, is not guaranteed or endorsed by the publisher.